AE International – North America

Atmospheric Environment 38 (2004) 2627–2638

ATMOSPHERIC ENVIRONMENT

www.elsevier.com/locate/atmosenv

Simulating regional-scale ozone climatology over the eastern United States: model evaluation results

C. Hogrefe[a,c,*], J. Biswas[a], B. Lynn[b], K. Civerolo[c], J.-Y. Ku[c], J. Rosenthal[b], C. Rosenzweig[d], R. Goldberg[d], P.L. Kinney[b]

[a] *Atmospheric Sciences Research Center, University at Albany, 251 Fuller Road, Albany, NY 12203, USA*
[b] *Mailman School of Public Health, Columbia University, 60 Haven AV., New York, NY 10032, USA*
[c] *Bureau of Air Quality Analysis and Research, New York State Department of Environmental Conservation (NYSDEC), 625 Broadway, Albany, NY 12233-3259, USA*
[d] *NASA Goddard Institute for Space Studies, 2880 Broadway, New York, NY 10025, USA*

Received 29 September 2003; accepted 13 February 2004

Abstract

To study the potential impacts of climate change on air quality and public health over the eastern United States, a coupled global/regional-scale modeling system consisting of the NASA-Goddard Institute for Space Studies Atmosphere–Ocean model, the MM5 mesoscale meteorological model and the Community Multiscale Air Quality (CMAQ) model for air quality has been developed. Evaluation results of the modeling system used to simulate climate and ozone air quality over the eastern United States during the five summers of 1993–1997 are presented in this paper. The results indicate that MM5 and CMAQ capture interannual and synoptic-scale variability present in surface temperature and ozone observations in the current climate, while the magnitude of fluctuations on shorter time scales is underestimated. A comparison of observed and predicted spatial patterns of daily maximum ozone concentrations shows best performance in predicting patterns for average and above-average ozone concentrations. The frequency distributions of the duration of extreme heat and ozone events show similar features for both model predictions and observations. Finally, application of a synoptic map-typing procedure reveals that the MM5/CMAQ system succeeded in simulating the average ozone concentrations associated with several frequent pressure patterns, indicating that the effects of synoptic-scale meteorology on ozone concentrations are captured by the modeling system. It is concluded that the GCM/MM5/CMAQ system is a suitable tool for the simulation of summertime surface temperature and ozone air quality conditions over the eastern United States in the present climate.

Keywords: Regional-scale air quality modeling; Model evaluation; Regional climate modeling; Interannual variability; Map-typing analysis

1. Introduction

Photochemical models systems such as CAMx (Morris, 2002) or Community Multiscale Air Quality (CMAQ) (Byun and Ching, 1999) have been used to simulate ozone concentrations under present day meteorological conditions with either current emissions or emissions that reflect emission control policies (Tesche and McNally, 1991; Kasibhatla and Chameides, 2000; Bouchet et al., 1999; Sistla et al., 2001). In recent years, there has been a growing interest in assessing the potential impact of climate change on air pollution and, ultimately, the public health impacts of both changing climate and air quality (McCarthy et al.,

*Corresponding author. Tel.: +1-518-402-8402; fax: +1-518-402-9035.
E-mail address: chogrefe@dec.state.ny.us (C. Hogrefe).

1352-2310/$ - see front matter © 2004 Elsevier Ltd. All rights reserved.
doi:10.1016/j.atmosenv.2004.02.033

2001). Climate change can influence the concentration and distribution of air pollutants through a variety of direct and indirect processes, including the modification of biogenic emissions, the change of chemical reaction rates, mixed-layer heights that affect vertical mixing of pollutants, and modifications of synoptic flow patterns that govern pollutant transport.

This paper and several other papers (Lynn et al., 2004a, b) focus on the substantiation and applications of a modeling study for simulating the effects of global climate change on regional climate and air quality over the northeastern United States in order to project the associated public health impacts in the region. A unique feature of this study is the linking of a regional mesoscale model with a global climate model. By using initial and boundary conditions from the global model to drive the regional climate model, this multi-component approach enables the elucidation of the effects of climate change on regional and urban scales which could not be obtained from the global simulations. The meteorological outputs from the mesoscale model simulations are subsequently used to simulate regional and urban air quality by coupling it to a photochemical model. Finally, results from both the meteorological and air quality-modeling simulations are coupled to health impact models to assess potential human health impacts of climate change. The health impact results will be presented in future works.

The primary objective of this paper is to evaluate the modeling system with observations in order to understand how well it simulates the present surface temperature and ozone concentrations on a regional scale and over the 31-county New York City metropolitan area, the region of interest of future health effects studies (Knowlton et al., 2003). Lynn et al. (2004a, b) have provided detailed information about how various configurations affect the regional climate model's ability to simulate mean meteorological parameters. In this study, we evaluate how well the models depicts both the average surface temperatures and ozone concentrations as well as their variability on different time scales as suggested in previous studies (US EPA, 1991; Biswas et al., 2001; Hogrefe et al., 2001a, b; Kunkel et al., 2002). In addition, we assess how well the regional climate and air quality models capture the frequency and length of high temperature and ozone events present in observations. This is of importance because extremes of summertime heat are thought to have a greater impact on human health than any other form of severe weather in the United States (Changnon et al., 1996). Further, by simulating multiple summers for the present climate conditions, the modeling system can be evaluated under different large-scale flow conditions as suggested by Anthes et al. (1989).

2. Models and database

2.1. Emissions processing

The county-level EPA 1996 National Emissions Trends (NET96) inventory was used as a basis for the air quality modeling. This emission inventory was processed by the Sparse Matrix Operator Kernel Emissions Modeling System (SMOKE) (Houyoux et al., 2000; Carolina Environmental Programs, 2003) to obtain gridded, hourly, speciated emission inputs for the air quality model. Temperature-dependent biogenic emissions were estimated by the Biogenic Emissions Inventory System—Version 2 (BEIS2) (Geron et al., 1994; Williams et al., 1992), while mobile source emissions were estimated by the Mobile5b model (US EPA, 1994) that takes into account the temperature dependence of fugitive emissions.

2.2. Global and regional climate modeling

Meteorological fields for the air quality simulations were obtained by coupling the MM5 mesoscale model (Grell et al., 1994) to the Goddard Institute for Space Studies (GISS) $4^\circ \times 5^\circ$ resolution Global Atmosphere–Ocean Model (GISS-GCM) (Russell et al., 1995). Details on the setup of this modeling system are described in Lynn et al. (2004a, b), thus, only a brief overview is presented here. In this study, we utilize MM5 simulations driven by GISS-GCM through boundary and initial condition inputs that were performed for the summer seasons (June–August) from 1993 to 1997. The MM5 was applied in a nested-grid mode with an inner grid having a horizontal resolution of 36 km over the eastern United States and an outer grid having a horizontal resolution of 108 km covering most of the continental United States; only results from the 36 km simulation were used in this study to perform the air quality simulations. The MM5 had 35 vertical layers, the height of the first layer was approximately 70 m. Lynn et al. (2004a) tested several different combinations of MM5 physics options, in this study we selected the MM5 simulations that were performed with the MRF boundary layer scheme (Hong and Pan, 1996), the Betts–Miller cloud scheme (Betts, 1986), the RRTM radiation scheme (Mlawer et al., 1997), and the Reisner2 microphysics scheme (Reisner et al., 1998).

2.3. Air quality modeling

Using the SMOKE-processed emissions and the 36 km MM5 regional climate simulation for the five summer seasons in the years 1993–1997, air quality simulations were performed using version 4.2 of the CMAQ model (Byun and Ching, 1999). The modeling domain consists of 68×59 horizontal and 16 vertical

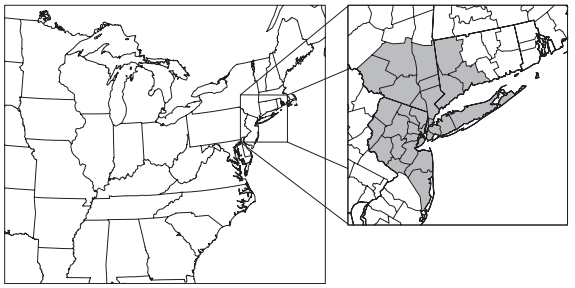

Fig. 1. Map of the 36 km CMAQ modeling domain. The 31-county region around New York City is highlighted in the insert.

grid cells and is depicted in Fig. 1. The insert in this figure highlights the 31-county region around New York City that is the focus of the public health impact research of this project. The Carbon Bond IV Mechanism (CB-IV) (Gery et al., 1989) was used to simulate gas phase chemistry, and time-invariant climatological profiles for ozone and its precursors were used as boundary conditions.

2.4. Observations

Hourly surface observations of meteorological variables were retrieved from the Data Support Section at the National Center for Atmospheric Research (NCAR-DSS). There were 258 monitors in the entire modeling domain and 18 in the greater New York City area that have at least 75% non-missing temperature observations for each of the summers from 1993 to 1997. Further, we utilized gridded sea level pressure fields from the archived ETA analysis (Black, 1994; Rogers et al., 1995, 1996) to evaluate MM5-simulated pressure patterns. The ETA analysis fields used here are archived at a horizontal resolution of 40 km and were regridded to the 36 km MM5 domain used in this study. Daily pressure fields at 1200 UTC were retrieved for 1996–2001 from NCAR. Additionally, we obtained hourly surface ozone observations for 1993–1997 from the EPA's AIRS system for 428 monitors located in the modeling domain shown in Fig. 1; 21 of these monitors are located in the greater New York City area. Analyses presented in this paper are based on both hourly and daily maximum observations and model predictions. For this purpose, model predictions were interpolated to the location of monitoring stations using bilinear interpolation.

2.5. Methods of analysis

2.5.1. Estimation of variability

Since MM5 was driven only by boundary conditions from a prediction-mode GISS-GCM simulation rather than being nudged towards observation-based reanalysis fields such as NCEP, fluctuations in observations and model predictions cannot be compared on a day-to-day or year-to-year basis. In other words, since the GCM is designed to simulate climate conditions over entire decades rather than reproduce observed meteorology on a given day of a specific year within a decade, the MM5 and CMAQ predictions for, say, 1 June 1993 are not designed to represent the actual observed conditions on that day. Hence, model evaluation techniques such as time series analysis of hourly observations and model-predicted values and scatter plots which seek a one-to-one correspondence between model simulations and temporally coinciding observed values could not be applied in this study. Consequently, some of the evaluation methods used in this study are aimed at measuring the modeling system's ability to capture spatio-temporal patterns of variability that are observed during five consecutive summer seasons in the 1990s. Specifically, these methods include the comparison of cumulative distribution functions (CDFs), the variances of observed and model simulated data on different time scales, and average spatial patterns under different synoptic flow regimes.

2.5.2. Spectral decomposition

An additional method of comparing observed and predicted variations is the use of spectral decomposition techniques as described in Hogrefe et al. (2000). To this end, time series of hourly meteorological and ozone concentrations are spectrally decomposed into intra-day (time period <12 h), diurnal (12–48 h), synoptic (2–21 days) and baseline (>21 days) components for each of the five summer seasons using the Kolmogorov–Zurbenko (KZ) filter as described in Hogrefe et al. (2000). The model analyses in this study consists of looking at the observed and modeled data on multiple temporal scales for entire summer season for all the 5 years to judge whether the model is able to replicate observed variability in temperature and ozone concentrations on different time scales.

2.5.3. Synoptic typing analysis

To identify common sea-level pressure patterns in the observations and their relation to both observed and predicted ozone concentrations, a correlation-based map-typing procedure (Lund, 1963; Kirchhofer, 1973) was used. The procedure is aimed at defining groups of days with similar pressure patterns; the frequency of occurrence of each of these groups is then determined and the most frequent groups are deemed to give a good representation of the typical pressure patterns in the gridded data set. Details on the procedure can be found in Yarnal (1993) and McKendry et al. (1995); the technique has also been discussed and applied by Lynn et al. (2004a) to compare pressure patterns predicted by

the GISS-GCM and several MM5 configurations to ETA analysis fields. In this study, we computed the observed and predicted ozone concentrations associated with three of the most frequent observed surface pressure patterns determined from the ETA analysis fields in an effort to evaluate the coupled meteorological/photochemical modeling system.

3. Results and discussion

3.1. Regional climate model evaluation

Because of its effect on biogenic emissions and chemical reactions rates as well as its impact on public health, the main focus of the MM5 evaluation is on the prediction of surface temperature. Additional meteorological fields, including winds, clouds, precipitation, moisture and radiation were compared against observations by Lynn et al. (2004a, b). Lynn et al. (2004a) reported that the MM5 simulation used in this study generally predicted mean spatial temperature patterns well, but tended to over predict temperatures in the southern portion of the modeling domain. Here, we expand their analysis by evaluating how well the model captures different aspects of variability present in the observations. Fig. 2 depicts the CDFs of daily maximum values of observed and MM5 predicted temperatures at all the observed sites in the modeling domain for all the 5 years analyzed in this study, each year represented by a separate curve. Descriptive parameters of these distributions are listed in Table 1. Data presented in Fig. 2 and Table 1 indicate that MM5 tends to slightly underestimate low and median daily maximum temperature values, while the 97.5th percentile is overestimated. This greater spread of model-predicted daily maximum temperatures compared to observations is consistent with a slight overestimation of total variance as shown in Table 1. Because each curve is constructed from daily maximum temperatures at 258 stations over 3 months, the variance of each curve is a measure of both spatial gradients in mean temperature and synoptic-scale temporal fluctuations. Lynn et al. (2004a) showed that MM5 tends to underestimate daily maximum temperature values in the northern part of the modeling domain and overestimate daily maximum temperature values in the southern part of the modeling domain; thus, the overestimation of variance of the CDFs shown in Fig. 1 is at least partially attributable to the overestimation of spatial gradients. Table 1 further illustrates that—for any given quantity such as the median or variance—the interval spanned by the lowest and highest predicted value overlaps the interval spanned by the lowest and highest observed value over the five summers for that quantity. Furthermore, the observed interannual variability of daily maximum values is captured as indicated by the similar magnitude of the interval spanned by the lowest and highest predicted and observed values over the five summers for any quantity. When the variances of the five observed and predicted median values are computed (Table 1) and subjected to an F-test, the null hypothesis that the two variances are equal cannot be rejected at a confidence level of 95%. These results imply that MM5 captures the range of temperature fluctuations caused by changing meteorological systems such as stagnant high pressure systems or frontal systems

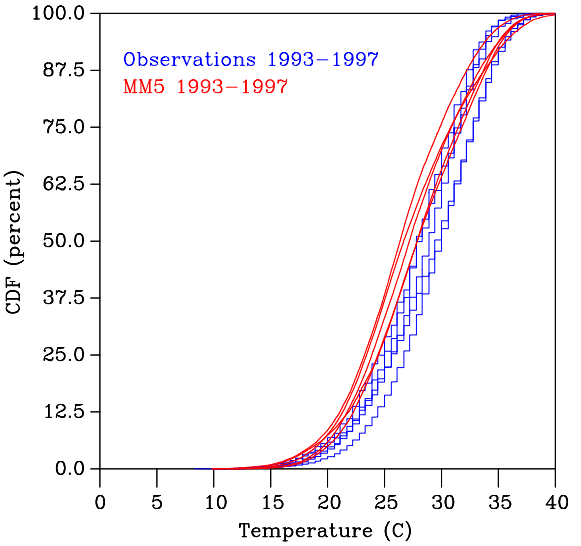

Fig. 2. CDFs of summertime daily maximum temperatures for the observed and modeled summers of 1993–1997 over the entire modeling domain. Each individual curve represents temperatures for one summer.

Table 1
Parameters of the observed and predicted cumulative distribution functions of domain-wide daily maximum temperature for the summers from 1993 to 1997 depicted in Fig. 2

	Observations	MM5
Mean (lowest/highest) (°C)	27.3/29.3	26.2/27.7
Variance (lowest/highest) (°C)^2	17.8/27.5	23.6/27.7
Median (lowest/highest) (°C)	27.8/29.4	26.1/27.5
2.5th Percentile (lowest/highest) (°C)	17.2/19.4	16.3/18.3
25th Percentile (lowest/highest) (°C)	23.9/26.7	22.9/24.1
75th Percentile (lowest/highest) (°C)	30.6/32.8	29.6/31.5
97.5th Percentile (lowest/highest) (°C)	34.4/36.7	35.2/37.2
Variance of five annual median values (°C)^2	0.39	0.36

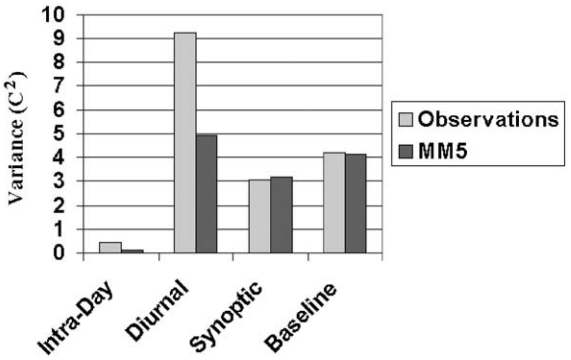

Fig. 3. Variance of the intra-day, diurnal, synoptic and baseline time series estimated from observed and modeled temperatures, spatially averaged over the entire modeling domain.

passages as well as the range of interannual temperature fluctuations.

An assessment of the model's ability to capture temperature variability on different temporal scales is presented in Fig. 3. The bars represent the amount of variance of the observed and predicted intra-day, diurnal, synoptic and baseline components that were estimated from hourly time series as described in Section 2.5.2. It can be seen that the variance of the longer-term fluctuations (i.e. the synoptic and baseline scales) is well captured by MM5, while the variance of shorter-term fluctuations on the intra-day and diurnal scales is underestimated. This is consistent with the results presented above. An analysis performed over the New York City region (figure not shown) showed similar results.

As stated above, MM5 was used in this modeling study to downscale meteorological fields from the GISS-GCM. While an in-depth comparison of GISS-GCM and MM5 simulations is provided in Lynn et al. (2004a), in this study we compare the synoptic and baseline scale variance predicted by both model and in the observations (intra-day and diurnal variance could not be computed because GCM fields were not available hourly). Results show that the variance of the GISS-GCM predicted synoptic component is less than one-third of that of the observed synoptic component, while MM5 captures the variance (figure not shown). The variance on the baseline scale is captured by both the GISS-GCM and the MM5. Thus, the successful simulation of synoptic-scale variability is a key benefit of using MM5 rather than the GISS-GCM in the current modeling study. When this analysis was performed for wind speed, results again showed that MM5 was able to capture the variances of fluctuations on longer time scales (synoptic and baseline), while underestimating the variance of intra-day and diurnal fluctuations. These findings are consistent with those of Hogrefe et al. (2001a), who analyzed two summertime simulations performed with the RAMS3b and MM5 models over the eastern United States.

From a health perspective, it is important to determine the number of consecutive days above certain temperature thresholds, i.e. the persistence of heat waves. While the CDFs discussed above show that MM5 captures the frequency of occurrence of high temperature events, we will now assess its ability to simulate the persistence of such events. Because of the latitudinal temperature gradients and human adaptation to these gradients, we define extreme heat events as days above the 90th percentile of observed and predicted daily maximum temperatures at any given site rather than as days above a fixed threshold such as 30°C. We then computed the length of each such extreme heat event and constructed a histogram of the relative frequency of the duration (in days) of such events for both observations and MM5 predictions. The results are depicted in Figs. 4a and b for stations in the entire domain and for the New York City area, respectively. Fig. 4a shows that the decrease of the relative frequency with increasing episode duration is reproduced by MM5. Both observations and model predictions show that slightly more than 50% of all extreme heat events are

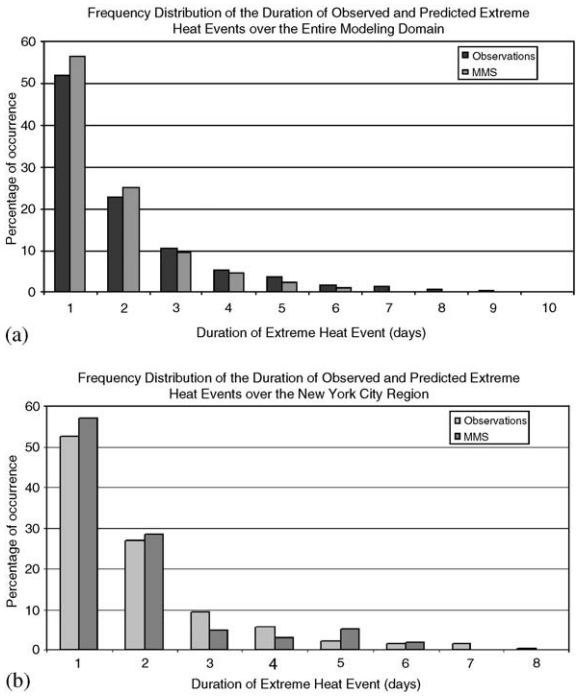

Fig. 4. Frequency distributions of the duration of observed and predicted extreme heat events. Results are shown for the entire modeling domain (a) and the New York City region (b). Extreme heat events are defined for each station as days exceeding the observed 90th percentile at that station.

single day events, and roughly 90% of all extreme heat events last 4 days or less. On the other hand, there was a small percentage of extreme heat events that last for 5 days and more, and MM5 was able to capture the frequency of occurrence of such events as well. However, it should be noted that the minor differences between the observed and predicted frequency distribution of the duration of extreme heat events visible in Fig. 4a are statistically significant at the 95% when subjected to a Kolmogorov–Smirnov test. Results for the New York City Region (Fig. 4b) show similar features and model performance, but because of the smaller sample size, the differences between the observed and predicted distributions are not statistically significant at the 95% confidence level.

3.2. Air quality model evaluation

Before evaluating CMAQ's ability to capture the variability embedded in ozone observations, a map of observed and predicted daily maximum 1-h ozone concentrations averaged over all simulated days during the years 1993–1997 was constructed and is presented in Fig. 5. It can be seen that the spatial pattern of mean daily maximum ozone concentrations is captured rather well. Bands of high average ozone concentrations are observed and predicted along the Ohio River valley and in an area stretching from northern Alabama and Georgia to central North Carolina and along the eastern seaboard. The spatial extent of mean ozone concentrations in excess of 55 ppb is also captured well. Fig. 5c shows that CMAQ slightly underestimates mean daily maximum ozone concentrations along the eastern seaboard, while it tends to have a small positive bias in the central portion of the modeling domain. Differences between observed and predicted average daily maximum O_3 concentrations rarely exceed 15 ppb. The correlation coefficient between the observed and predicted average daily maximum ozone concentrations at all 428 stations is 0.68, while the bias is <1 ppb and the root mean square error is 6 ppb. For average daily maximum 8-h ozone concentrations, the correlation coefficient is 0.62, while the bias is 4 ppb and the root mean square error is 7 ppb.

After having compared observed and predicted mean daily maximum ozone concentrations, we now aim at evaluating how well CMAQ is able to capture the variability embedded in ozone observations. Figs. 6a and b show the CDFs for observed and predicted 1- and 8-h daily maximum ozone concentrations for the entire domain for the five summers simulated, and Tables 2a and b list some of the parameters describing the depicted distributions. CMAQ overestimates low values for both 1- and 8-h daily maximum ozone concentration; high values are underestimated for 1-h concentrations and captured for 8-h concentrations. As a result, the

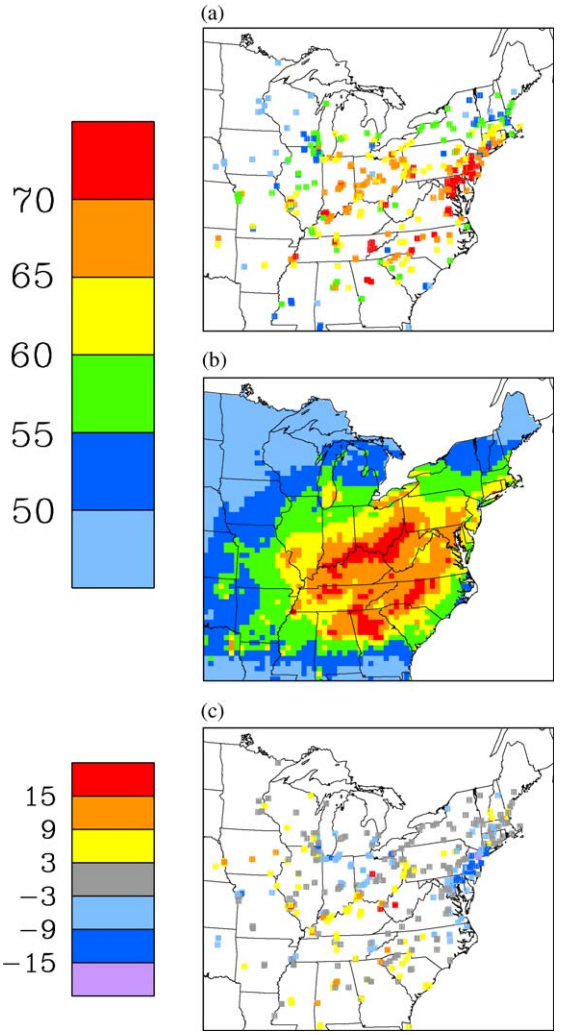

Fig. 5. Observed (a) and CMAQ-predicted (b) 1-h daily maximum ozone concentrations, averaged over all summer days from 1993 to 1997. Panel (c) shows the difference between CMAQ-predicted and observed average 1-h daily maximum ozone concentrations.

variance of the predicted distributions of both 1- and 8-h daily maximum ozone concentrations is lower than that of the observed distributions. The interval between the lowest and highest annual value of any given quantity in Tables 2a and b is comparable for observations and model predictions, indicating that the interannual variability of the observed ozone distributions is largely captured. When the variances of the five observed and predicted median values are computed (Tables 2a and b) and subjected to an F-test, the null hypothesis that the two variances are equal cannot be rejected at a confidence level of 95%.

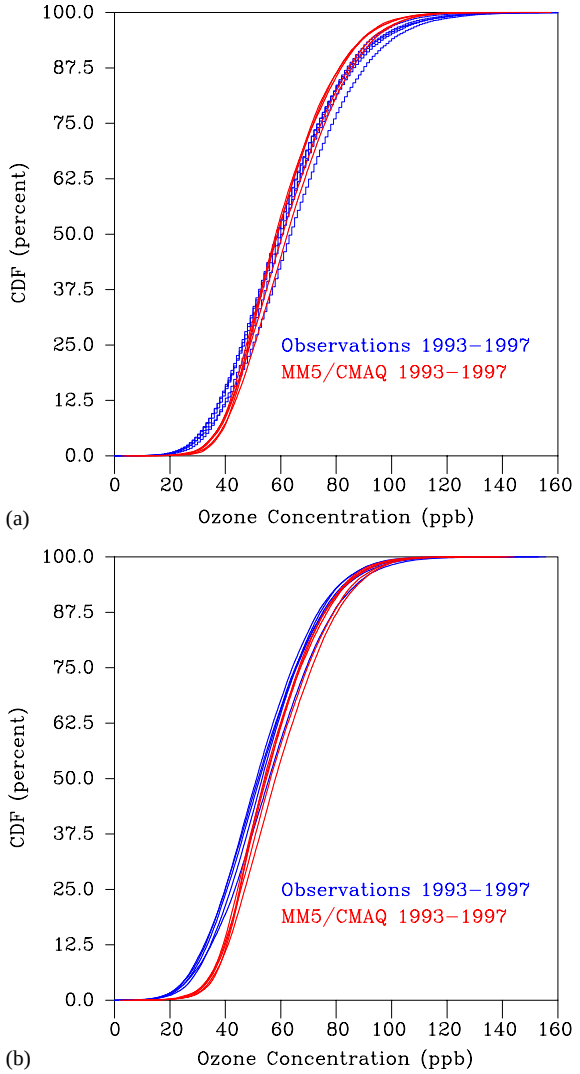

Fig. 6. CDFs of summertime daily maximum 1-h (a) and 8-h (b) ozone concentrations for the observed and modeled summers of 1993–1997 over the entire modeling domain. Each individual curve represents ozone concentrations from one summer.

Table 2
Parameters of the observed and predicted cumulative distribution functions of domain-wide daily maximum ozone concentrations for the summers from 1993 to 1997

	Observations	CMAQ
(a) 1-h daily maximum ozone concentrations depicted in Fig. 7a		
Mean (lowest/highest) (ppb)	60.8/65.2	60.5/64
Variance (lowest/highest) $(ppb)^2$	362/468	273/328
Median (lowest/highest) (ppb)	59/64	58/62
2.5th Percentile (lowest/highest) (ppb)	27/29	33/35
25th Percentile (lowest/highest) (ppb)	46/50	48/51
75th Percentile (lowest/highest) (ppb)	74/79	71/76
97.5th Percentile (lowest/highest) (ppb)	102/111	97/102
Variance of five annual median values $(ppb)^2$	3.4	2.4
(b) 8-h daily maximum ozone concentrations depicted in Fig. 7b		
Mean (lowest/highest) (ppb)	53/57	57/60
Variance (lowest/highest) $(ppb)^2$	290/365	240/287
Median (lowest/highest) (ppb)	51/56	54/58
2.5th Percentile (lowest/highest) (ppb)	22/24	30/32
25th Percentile (lowest/highest) (ppb)	40/43	44/47
75th Percentile (lowest/highest) (ppb)	64/69	66/71
97.5th Percentile (lowest/highest) (ppb)	90/97	90/96
Variance of five annual median values $(ppb)^2$	2.5	2.2

The CDFs analyzed above depict variability introduced by both temporal fluctuations and spatial gradients of observed and predicted 1- and 8-h daily maximum ozone concentrations. To separately assess the model's ability to capture spatial patterns, distribution functions of observations and predictions were generated separately for each monitor, and 460 spatial maps were constructed from these functions. The first map corresponds to the lowest observed and predicted daily maximum ozone concentrations over the five summer period at any given monitor (i.e. a map of the 1/460th percentile), the second map corresponds to the second lowest concentration (i.e. a map of the 2/460th percentile), and so on. By computing the correlation coefficient, bias and root mean square error between the observed and predicted maps for a given percentile, the model's ability to reproduce spatial patterns under different situations can be evaluated. Results of this analysis are presented in Table 3. The correlation coefficients indicate that the spatial patterns are captured best for intermediate and high percentiles, while there is little correlation between the spatial maps of very low observed and predicted concentrations. The root mean square error of the predicted patterns is <10 ppb except for very low and high percentiles. In the case of 1-h daily maximum ozone concentrations, the bias is close to zero for intermediate percentiles, while low observations tend to be overpredicted and high observations tend to be underpredicted. In the case of 8-h daily maximum ozone concentrations, the bias decreases steadily with increasing percentiles. Overall, these results indicate that the model exhibits skill in

Table 3
Correlation coefficient R, bias and root mean square error between the observed and predicted maps for a given percentile of the daily maximum 1- and 8-h ozone concentrations

	1-h daily maximum			8-h daily maximum		
	R	Bias (ppb)	RMSE (ppb)	R	Bias (ppb)	RMSE (ppb)
2.5th percentile	0.28	7.9	10.2	0.23	11.5	13.3
25th percentile	0.59	2.3	6.7	0.5	6.0	8.7
50th percentile	0.69	0.1	6.4	0.63	4.0	7.7
75th percentile	0.76	−1.3	6.4	0.71	3.5	7.3
97.5th percentile	0.75	−7.1	11.3	0.66	1.0	8.2

Note: To calculate these statistics, a total of 460 daily maps were constructed, where the first map consisted of the lowest observed and predicted daily maximum concentration at each monitor during the five summers considered, the 230th map showed the median observed and predicted daily maximum concentration at each monitor, and so on.

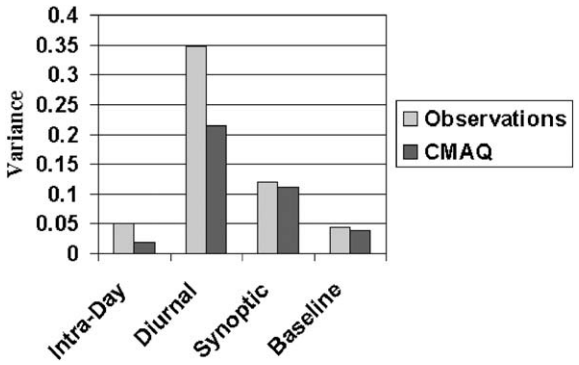

Fig. 7. Variance of the intra-day, diurnal, synoptic and baseline time series estimated from observed and modeled ozone concentrations, spatially averaged over the entire modeling domain.

capturing spatial patterns not only for the average conditions displayed in Fig. 5, but also for a wide range of conditions.

Furthermore, time series of hourly observed and predicted ozone concentrations were spectrally decomposed into different temporal components as described earlier. The bars in Fig. 8 represent the amount of variance of the observed and predicted intra-day, diurnal, synoptic and baseline components. As seen from the figure, the diurnal component is the largest contributor to the overall variance in both observations and model predictions. While CMAQ strongly underestimates the strength of fluctuations on the intra-day and, to a lesser extent, the diurnal time scale, it only slightly underestimates the strength of the longer-term fluctuations on the synoptic and baseline scales. In summary, the results presented in Figs. 5–7 indicate that the CMAQ simulations are able to capture the regional-scale ozone climatology and longer-term fluctuations, while increased horizontal and vertical grid resolution presumably would be necessary to better represent the entire range of meteorological and ozone fluctuations on shorter time scales, especially in urban areas. These results are consistent with Bouchet et al. (1999), who demonstrated that model-predicted results of ozone exceedances agree better with observations for longer time periods, thus proving the feature of current-generation modeling systems to better capture broader-based longer-term events rather than transient, smaller-scale features.

As in the case of temperature, we also assessed CMAQ's ability to reproduce the frequency distribution of the duration of extreme ozone events. However, rather than using a station-dependent definition of 'extreme event' (for temperature, the 90th percentile of observed daily maximum temperature was used as threshold to account for latitudinal temperature gradients and human adaptation to such gradients), we defined extreme ozone events as days exceeding 120 and 80 ppb for 1- and 8-h daily maximum ozone concentrations, respectively. The results from this analysis are depicted in Figs. 8a and b for the entire domain. It is evident that 1-h concentrations above 120 ppb are usually 1-day events, with hardly any occurrences of such extreme events lasting longer than 3 days. CMAQ reproduces this feature. Both observations and CMAQ show that there is a higher frequency of occurrence of episodes on which 8-h ozone concentrations exceed 80 ppb for at least 3 days compared to 1-h concentrations. Again, CMAQ captures the shape of the frequency distribution, although is has to be noted that the minor differences between the observed and predicted frequency distributions visible in Fig. 8b are statistically significant at the 95% when subjected to a Kolmogorov–Smirnov test. Since persistence of high ozone concentrations is typically driven by meteorological conditions such as stagnating high pressure systems and persistent low wind speeds in the boundary layer (Ghim et al., 2001), this result is a further indication that

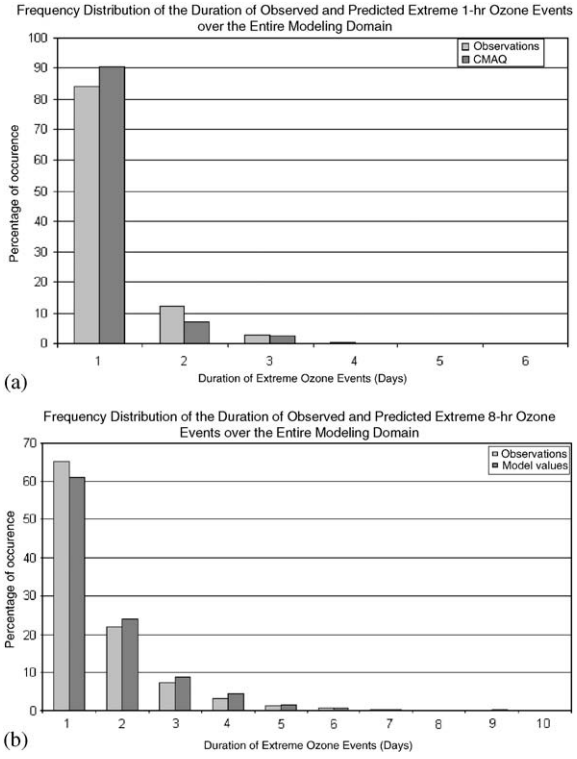

Fig. 8. Frequency distributions of the duration of observed and predicted extreme ozone events over the entire modeling domain. Results are shown for extreme 1-h ozone events (i.e. days with daily maximum 1-h ozone concentrations exceeding 120 ppb) in panel (a) and for extreme 8-h ozone events (i.e. days with daily maximum 8-h ozone concentrations exceeding 80 ppb) in panel (b).

the MM5/CMAQ modeling system is capturing the weather-induced variations of ground-level ozone concentrations.

3.3. Air quality model evaluation using synoptic patterns

Surface ozone concentrations depend on complex combinations of precursor emission patterns, chemical transformations and meteorological influences. Despite this complex relationship, we attempted to elucidate the relationship between different synoptic pressure regimes and observed ozone concentrations and to evaluate whether the MM5/CMAQ modeling system captures these relationships. To this end, we employed the correlation-based Kirchhofer synoptic typing technique described in Section 2.5.3. Using this method, Lynn et al. (2004a) showed that the various configurations of the GCM/MM5 are able to adequately represent the range of synoptic patterns present in observations. In this study, we identified the three most frequently observed sea level pressure patterns, and determined the average observed and predicted ozone concentrations over all days that were identified by the Kirchhofer procedure to be represented by any of these three patterns. The nine panels in Fig. 9 show the result of this analysis; the three most frequent sea level pressure patterns are shown in panels (a), (d) and (g), the associated observed ozone patterns in panels (b), (e) and (h), and the associated CMAQ-predicted ozone patterns in panel (c), (f) and (i). The three most frequent pressure patterns are the Bermuda high (Fig. 9a), a high pressure system over the northeast quadrant of the modeling domain coupled with a trough oriented along the east coast (Fig. 9d), and a high pressure system centered over New England (Fig. 9g). For the Bermuda high pressure pattern, both observations (Fig. 9b) and model predictions (Fig. 9c) show high ozone concentrations over large portion of the Northeast, facilitated by the southwesterly flow pattern that allows air masses to pick up fresh emissions as they travel over land. The correlation between the averaged observed and predicted ozone concentrations for this pattern over 428 stations is 0.74. In contrast, high observed (Fig. 9e) and predicted (Fig. 9f) ozone concentrations associated with the second pressure pattern are restricted to the southern portion of the modeling domain, reflecting the inflow of cleaner air into the northern part of the modeling domain caused by the northwesterly winds to the west of the trough. The correlation between the averaged observed and predicted ozone concentrations for this second pattern is 0.75. Finally, ozone concentrations associated with the high pressure system centered over New England show maxima over the Midwestern states, while ozone concentrations along the coastline are low because of the general onshore flow (Figs. 9h and i), and the correlation between the averaged observed and predicted ozone concentrations for this pattern is 0.73. In summary, the MM5/CMAQ system captures the mean ozone concentrations associated with frequent pressure patterns well, indicating that both the mean emission patterns and the effects of synoptic-scale meteorology on ozone concentrations are well represented in the modeling system.

4. Summary

This paper described the evaluation of a coupled global/regional modeling system used to simulate climate and ozone air quality over the eastern United States during the five summers of 1993–1997. The system consisted of the GISS-GCM, the MM5 mesoscale model and the CMAQ model to simulate air quality. Model evaluation focused on determining how well the modeling system captured the variability embedded in surface temperature and ozone observations for several years under different meteorological conditions.

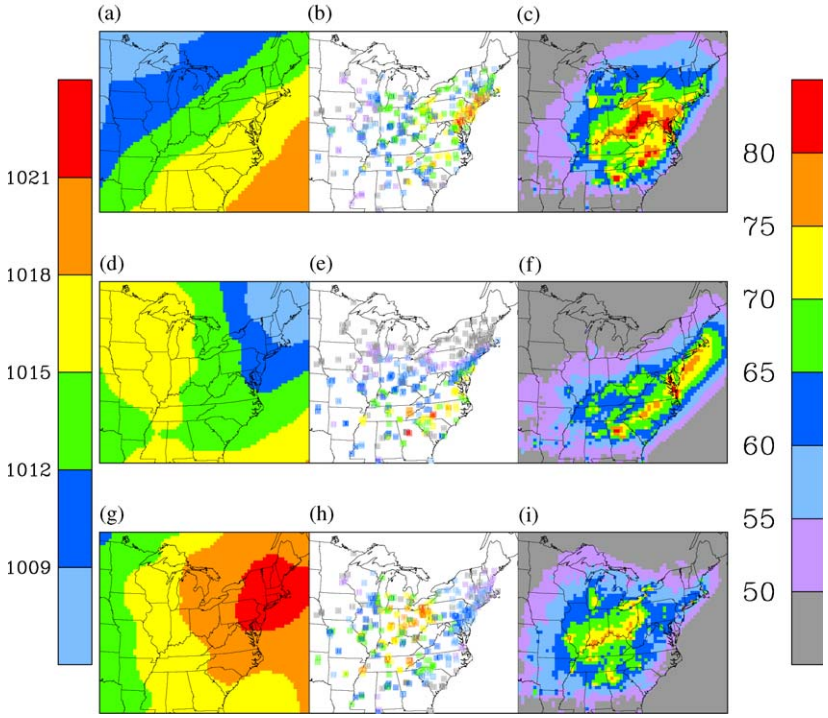

Fig. 9. Three most frequently observed sea level pressure pattern (panels a, d and g), associated observed ozone patterns in panels (panels b, e and h) and associated CMAQ-predicted ozone patterns (panels c, f and i). Pressure is shown in mbar, while ozone concentrations are shown as ppb.

The results indicated that MM5 and CMAQ captured interannual and synoptic-scale variability present in surface temperature and ozone observations in the current climate, while the magnitude of fluctuations on the intra-day and diurnal time scales was underestimated. A comparison of observed and predicted spatial pattern of daily maximum ozone concentrations shows best performance in predicting patterns for average and above-average ozone concentrations. The shape of the frequency distribution of the duration of extreme heat events was captured by MM5 over the entire modeling domain as well as for the New York City area. The features of the frequency distribution of extreme ozone event durations were reproduced by CMAQ for both 1- and 8-h daily maximum concentrations. Finally, application of a synoptic map-typing procedure revealed that the MM5/CMAQ system succeeded in simulating the mean ozone concentrations associated with several frequent pressure patterns, indicating that the effects of synoptic-scale meteorology on ozone concentrations are captured by the modeling system.

In summary, the results suggest that the GCM/MM5/CMAQ system is a suitable tool for the simulation of summertime surface temperature and ozone air quality over the eastern United States in the present climate. Future applications of this modeling system will include simulations under future climate scenarios to assess the effect of global climate change on regional-scale air quality, simulations examining the efficacy of United States emission control strategies under various climate scenarios, and higher resolution simulations to assess the health impacts of both land use and climate change in the New York City metropolitan area.

Acknowledgements

This work was supported by the US Environmental Protection Agency under STAR grant R-82873301.

Disclaimer

Although the research described in this article has been funded in part by the US Environmental Protection Agency, it has not been subjected to the Agency's required peer and policy review and therefore does not necessarily reflect the views of the Agency and no official endorsement should be inferred.

References

Anthes, R.A., Kuo, Y.H., Hsie, E.Y., Low-Nam, S., Bettge, T.W., 1989. Estimation of skill and uncertainity in regional numerical models. Quarterly Journal of the Royal Meteorological Society 115, 763–806.

Betts, A.K., 1986. A new convective adjustment scheme. Part I: observational and theoretical basis. Quarterly Journal of the Royal Meteorological Society 112, 677–692.

Biswas, J., Hogrefe, C., Rao, S.T., Hao, W., Sistla, G., 2001. Evaluating the performance of regional-scale photochemical modeling systems. Part III—precursor predictions. Atmospheric Environment 35, 6129–6149.

Black, T.L., 1994. The new NMC mesoscale eta model: description and forecast examples. Weather and Forecasting 9, 265–278.

Bouchet, V.S., Laprise, R., Torlaschi, E., 1999. Studying ozone climatology with a regional climate model: 2. Climatology. Journal of Geophysical Research 104, 30373–30385.

Byun, D.W., Ching, J.K.S. (Eds.), 1999. Science Algorithms of the EPA Models-3 Community Multiscale Air Quality Model (CMAQ) Modeling System. EPA/600/R-99/030, US Environmental Protection Agency, Office of Research and Development, Washington, DC 20460.

Carolina Environmental Programs, 2003. Sparse Matrix Operator Kernel Emission (SMOKE) Modeling System. University of Carolina, Carolina Environmental Programs, Research Triangle Park, NC.

Changnon, S.A., Kunkel, K.E., Reinke, B.C., 1996. Impact and responses to the 1995 heat wave: a call to action. Bulletin of the American Meteorological Society 77, 1497–1506.

Geron, C.D., Guenther, A.B., Pierce, T.E., 1994. An improved model for estimating emissions of volatile organic compounds from forests in the eastern United States. Journal of Geophysical Research 99, 12773–12791.

Gery, M.W., Whitten, G.Z., Killus, J.P., Dodge, M.C., 1989. A photochemical kinetics mechanism for urban and regional scale computer modeling. Journal of Geophysical Research 94, 12925–12956.

Ghim, Y.S., Oh, Y.S., Chang, Y.S., 2001. Meteorological effects on the evolution of high ozone episodes in the greater Seoul area. Journal of the Air and Waste Management Association 51, 185–202.

Grell, G.A., Dudhia, J., Stauffer, D., 1994. A description of the fifth-generation Penn State/NCAR Mesoscale Model (MM5). NCAR Technical Note, TN-398 + STR, National Center for Atmospheric Research, Boulder, CO, 138pp.

Hogrefe, C., Rao, S.T., Zurbenko, I.G., Porter, P.S., 2000. Interpreting the Information in ozone observations and model predictions relevant to regulatory policies in the eastern United States. Bulletin of the American Meteorological Society 81, 2083–2106.

Hogrefe, Rao, S.T., Kasibhatla, P., Kallos, G., Tremback, C., Hao, W., Olerud, D., Xiu, A., McHenry, J., Alapaty, K., et al., 2001a. Evaluating the performance of regional-scale photochemical modeling systems: Part I—meteorological predictions. Atmospheric Environment 35, 4159–4174.

Hogrefe, C., Rao, S.T., Kasibhatla, P., Hao, W., Sistla, G., Mathur, R., McHenry, J., 2001b. Evaluating the performance of regional-scale photochemical modeling systems: Part II—ozone predictions. Atmospheric Environment 35, 4175–4188.

Hong, S.-Y., Pan, H.-L., 1996. Nonlocal boundary layer vertical diffusion in a medium-range forecast model. Monthly Weather Review 124, 2322–2339.

Houyoux, M.R., Vukovich, J.M., Coats, Jr., C.J., Wheeler, N.J.M., Kasibhatla, P., 2000. Emission inventory development and processing for the seasonal model for regional air quality. Journal of Geophysical Research 105, 9079–9090.

Kasibhatla, P., Chameides, W.L., 2000. Seasonal modeling of regional ozone pollution in the eastern United States. Geophysical Research Letters 27, 1415–1418.

Kirchhofer, W., 1973. Classification of European 500 mb patterns. Arbeitsbericht der Schweizerischen Meteorologischen Zentralanstalt Nr. 43, Geneva.

Knowlton, K.M., Rosenthal, J.E., Gaffin, S., Rosenzweig, C., Goldberg, R., Lynn, B., Kinney, P.L., 2003. Modeling public health impacts of climate change in the New York metropolitan region. Fifth International Conference on Urban Climate, Lodz, Poland, 1–5 September 2003.

Kunkel, K.E., Andsager, K., Liang, X., 2002. Observations and regional climate model simulations of heavy precipitation events and seasonal anomalies: a comparison. Journal of Hydrometeorology 3, 322–334.

Lund, I.A., 1963. Map-pattern classification by statistical methods. Journal of Applied Meteorology 2, 56–65.

Lynn, B.H., Rosenzweig, C., Goldberg, R., Hogrefe, C., Rind, D., Dudhia, J., Druyan, L., Healy, R., Biswas, J., Kinney, P., Rosenthal, J., 2004a. The GISS-MM5 regional climate modeling system. Part I: sensitivity of simulated current and future climate to model configuration. Journal of Climate, submitted for publication.

Lynn, B.H., Rosenzweig, C., Goldberg, R., Hogrefe, C., Rind, D., Dudhia, J., Druyan, L., Healy, R., Kinney, P., Rosenthal, J., 2004b. The GISS-MM5 regional climate modeling system. Part II: sensitivity of simulated climate (and climate change) to cumulus parameterization and model grid resolution. Journal of Climate, submitted for publication.

McCarthy, J.J., Canziani, O.F., Leary, N.A., Dokken, D.J., White, K.S. (Eds.), 2001. Climate Change 2001: Impacts, Adaptation and Vulnerability. Intergovernmental Panel on Climate Change (IPCC). Cambridge University Press, New York, NY.

McKendry, I.G., Steyn, D.G., McBean, G., 1995. Validation of synoptic circulation patterns simulated by the Canadian Climate Center General Circulation Model for Western North America. Atmosphere–Ocean 33 (4), 809–825.

Mlawer, E.J., Taubman, S.J., Brown, P.D., Iacono, M.J., Clough, S.A., 1997. Radiative transfer for inhomogeneous atmosphere: RRTM, a validated correlated-k model for the longwave. Journal of Geophysical Research 102, 16663–16682.

Morris, R., 2002. Comprehensive Air Quality Model with Extension (CAMx), Version 3.1. ENVIRON International Corporation, 101 Rowland Way, Navato, CA 94945-5010.

Reisner, J., Rasmussen, R.J., Bruintjes, R.T., 1998. Explicit forecasting of supercooled liquid water in winter storms using the MM5 mesoscale model. Quarterly Journal of the Royal Meteorological Society 124B, 1071–1107.

Rogers, E., Black, T.L., DiMego, G.J., 1995. The regional analysis system for the operational "early" Eta model: original 80 km configuration and recent changes. Weather and Forecasting 10, 810–825.

Rogers, E., Black, T.L., Deaven, D.G., DiMego, G.J., Zhao, Q., Baldwin, M., Junker, N.W., Lin, Y., 1996. Changes to the operational "early" Eta analysis/forecast system and the National Centers for Environmental Prediction. Weather and Forecasting 11, 391–413.

Russell, G.L., Miller, J.R., Rind, D., 1995. A coupled atmosphere–ocean model for transient climate change studies. Atmosphere–Ocean 33, 683–730.

Sistla, G., Hao, W., Ku, J.-Y., Kallos, G., Zhang, K., Mao, H., Rao, S.T., 2001. An operational evaluation of two regional-scale ozone air quality modeling systems over the eastern United States. Bulletin of the American Meteorological Society 82, 945–963.

Tesche, T.W., McNally, D.E., 1991. Photochemical modeling of two 1984 SCCAMP ozone episodes. Journal of Applied Meteorology 30, 745–763.

US Environmental Protection Agency (US EPA), 1991. Guideline for regulatory applications of the Urban Airshed Model. Report of EPA-450/4-91-013, Research Triangle Park, NC.

US Environmental Protection Agency, 1994. User's guide to Mobile5 (Mobile source emission factor model). Report of EPA/AA/TEB/94/01, Ann Arbor, MI.

Williams, E.J., Guenther, A., Fehsenfeld, F.C., 1992. An inventory of nitric oxide emissions from soils in the United States. Journal of Geophysical Research 97 (D7), 7511–7519.

Yarnal, B., 1993. Synoptic climatology in environmental analysis: a primer. Bellhaven Press, London, UK, 195pp.